tvst

Article

Distinct Nuclear Architecture of Photoreceptors and Light-Induced Behaviors in Different Strains of Mice

Mingxue Zhou[1], Yutong Liu[2], and Chao Ma[3]

[1] Beijing Hospital of Traditional Chinese Medicine, Capital Medical University, Beijing Institute of Traditional Chinese Medicine, Beijing, China
[2] State Key Laboratory of Biomembrane and Membrane Biotechnology, School of Life Sciences, Tsinghua University, Beijing, China
[3] Radboud Institute for Molecular Life Sciences, Radboud University Medical Center, Nijmegen, The Netherlands

Correspondence: Chao Ma, Radboud Institute for Molecular Life Sciences, Radboud University Medical Center, 6500HB, Nijmegen, The Netherlands. e-mail: chaomabiomed@gmail.com

Received: June 30, 2020
Accepted: January 22, 2021
Published: February 25, 2021

Keywords: nuclear architecture; rod; cone; light-dark behavior; retina

Citation: Zhou M, Liu Y, Ma C. Distinct nuclear architecture of photoreceptors and light-induced behaviors in different strains of mice. Trans Vis Sci Tech. 2021;10(2):37, https://doi.org/10.1167/tvst.10.2.37

Purpose: The mouse retina is considered a remarkable model for studying gene functions. However, variations in genetic background influence phenotypes in the mammalian retina. Therefore this study aimed to investigate the effects of the genetic background on the nuclear architecture of photoreceptor cells and the light-induced behavior in C57BL/6, 129 × 1/svj, and ICR mice.

Methods: The nuclear architecture of photoreceptor cells was investigated using various staining methods on postnatal day 21 (P21). Murine behavior was observed using a light-dark compartment test.

Results: The outer nuclear layer and retina were significantly thicker in C57BL/6 mice than in 129 × 1/svj mice. The percentage of photoreceptors with one chromocenter was significantly higher in C57BL/6 mice than in 129 × 1/svj and ICR mice on P21. The numbers of photoreceptor cells in C57BL/6 and ICR mice were significantly higher than those in 129 × 1/svj mice. The behavior test revealed that the walking distance and velocity in the light compartment were increased in C57BL/6 and ICR mice compared to 129 × 1/svj mice.

Conclusions: Different mouse strains had a distinct nuclear architecture of photoreceptors on P21, and C57BL/6 and ICR mice were more active than 129 × 1/svj mice in response to light-induced stress.

Translational Relevance: This study demonstrates a technique for assessing retinal structures and nuclear architecture in various strains of mice, which are often used to model human retinal disease. Hence, this study may help to elucidate the effect of genetic or disease-induced variance in retinal architecture and the organization of photoreceptor nuclear content on visual function in humans.

Introduction

Duplex retinas, which consist of both rod and cone photoreceptors, are considered to exist in all vertebrates.[1,2] Mice have a rod-dominated retina; the percentage of cones is approximately 1% to 10% because of the nocturnal behavior of mice.[3–6] Furthermore, Solovei et al.[7] showed that the nuclear architecture of rod photoreceptor cells in nocturnal mammals is radically different from that in diurnal mammals. Rod photoreceptor cells of diurnal retinas have the conventional architecture with euchromatin located in the interior part of nuclei and heterochromatin resided in the periphery of the rod nuclei. By contrast, rods of nocturnal retinas have an inverted pattern with heterochromatin located in the nuclear center, whereas euchromatin is found near the nuclear border.[7]

Compared to euchromatin, heterochromatin is more condensed and predominantly located near the nuclear envelope and thus less available to transcription factors.[8,9] Although nuclear architecture in different cell types can significantly differ in detail, the abovementioned pattern is evolutionarily conserved from the unicellular to multicellular organisms.[7,10] The crucial role that the spatial arrangement of chromatin plays in

transcriptional regulation may account for the evolutionary stability of the nuclear architecture.[11,12] In the transcription process, genes at the nuclear periphery are repositioned to the interior where they are transcribed.[13] In light of the essential role of the nuclear architecture in regulating nuclear functions, the inverted pattern of the chromatin distribution in mouse rod photoreceptors can influence the transmission of light through the outer nuclear layer (ONL).[7] The rod photoreceptors work as collecting lenses that improve the optical transmission of the mouse retina.[7,14] Subramanian et al.[14] further demonstrated that the inverted nuclei with their forward scattering properties predominantly restrain light scattering by nuclear substructure towards large angles, thereby improving image veil and retinal contrast transmission.

The differences in the nuclear architecture of rod photoreceptor cells between diurnal and nocturnal mammals have been well documented.[7] Within a given species, the retinas of distinct subpopulations have different susceptibilities to fundus diseases, which is probably not only because the complex polygenic factors, epigenetics, or risk factors from other chronic conditions but also because the subtle differences in their retinal structure and function.[15–18] Friedman et al.[19] reported that more than 40 years old White people are more likely to have late age-related macular degeneration than age-matched Black people. Likewise, the genetic background has also been reported to affect light-induced retinal damage in both mice[20] and rats.[21,22] LaVail et al.[20] investigated the sensitivity to light-induced photoreceptor degeneration in seven different inbred strains of albino mice and found that different inbred strains of mice exhibited a broad range of sensitivities to light-damaging effects. Tremblay and colleagues compared the difference in protective effects of a blueberry-enriched diet on the retina exposed to bright light between albino Wistar and pigmented Brown Norway rats.[22] Their results showed that this dietary intervention protected albino Wistar rats' retina from light damage, whereas this did not occur in Brown Norway rats.[22] Comparing photoreceptor cell death after retinal detachment, Matsumoto et al.[23] reported that the genetic background exerted an influence on photoreceptor cell death after retinal detachment in C57BL/6, BALB/c, and B6129SF2 mice. They found that the inflammatory response, nerve growth factor expression, ratio of outer nuclear layer to inner nuclear layer, apoptotic and autophagic signaling, and inhibition of apoptosis-related proteins after retinal detachment differed significantly among these three inbred mouse strains.[23]

To date, possible differences in the nuclear architecture of photoreceptor cells and light-induced behavior among different mouse strains have not yet been investigated. Therefore we chose pigmented C57BL/6 mice and albino 129 × 1/svj and ICR mice, which are commonly used for gene-targeting research today. These mice differ in gene expression and behavioral phenotypes,[24,25] efficacy of physical exercise, adult neurogenesis,[26] numbers of retinal ganglion cells,[27] and fundus and retinal thickness.[28] The present study analyzed the differences in the thickness of the ONL and the whole retina, nuclear architecture of photoreceptor cells, and light-induced behavior among C57BL/6, 129 × 1/svj, and ICR mice to provide a solid theoretical basis and methodological reference for the phenotypic analysis of the visual system of these different mouse strains.

Materials and Methods

Animals

Male C57BL/6, 129 × 1/svj, and ICR mice were bred by the Animal Facility of Tsinghua University. All animal experiments were conducted according to relevant institutional guidelines and laws, and the animal care procedures were strictly in accordance with the regulations of the Institutional Animal Care and Use Committee of Tsinghua University. All study protocols adhered to the ARVO Statement for the Use of Animals in Ophthalmic and Vision Research.

Hematoxylin and Eosin and 3,3′-Diaminobenzidine Immunohistochemistry

The pattern differences between nocturnal and diurnal mammals regarding their nuclear architecture of rod cells have been investigated in detail.[7] However, little is known about the differences in the nuclear architecture of rod photoreceptors in different mouse strains. In the present study, the nuclear architecture of photoreceptor cells was compared among C57BL/6, 129 × 1/svj, and ICR mice. Mice open their eyes on postnatal day (P) 13, the retinas mature on P21, and sexual maturity is reached on P28.[7,29] Therefore the photoreceptor cells were assessed on P14, P21, P28, and at six weeks in C57BL/6, 129 × 1/svj, and ICR mice.

Mice were sacrificed, and their eyes were harvested on P14, P21, and P28, and at week six. The eyeballs were fixed in a fixative solution as reported earlier[30] (glacial acetic acid: formalin: 0.9% sodium chloride: 75% alcohol; 1:2:7:10) for 24 hours and embedded in paraffin. Then, 5 µm sections were cut, and

serial sections of 5 µm paraffin-embedded tissues were prepared. Paraffin sections were subsequently rehydrated in a descending series of ethanol concentrations (from 100% to 50%). Then, the eye tissue sections were placed in hematoxylin for one minute, rinsed in deionized water for five minutes, dipped in acid ethanol, rinsed in deionized water for two minutes, placed in eosin for 30 seconds, and rinsed in deionized water for another five minutes. Afterward, the tissues were dehydrated in an ascending series of ethanol concentrations (from 50% to 100%). Finally, the tissues were cleared in xylene and embedded in paraffin wax.

Two serial sections of 5 µm paraffin-embedded tissue were prepared to conduct 3,3′-diaminobenzidine (DAB) staining. DAB staining was performed as previously described.[30] The sections were incubated at 4°C overnight with the following primary antibodies: anti-M-opsin (1:500; Millipore, Burlington, MA, USA), anti-H3K4 (1:100; Sigma-Aldrich, St. Louis, MO, USA), anti-H3K9 (1:500; Sigma-Aldrich), and anti-H4K20 (1:1000; Sigma-Aldrich) antibodies.

Retinal Semi-Thin Sections

Retina pieces were fixed with 2.5% glutaraldehyde in 0.1 M phosphate buffer for one hour. Then, the retina pieces were rinsed, dehydrated with an ascending series of ethanol concentrations, and embedded in SPON12 resin. Semi-thin sections (0.5 µm) were prepared using a Leica EM UC7 microtome (Leica Microsystems, Wetzlar, Germany). The sections were stained with toluidine blue (Sigma-Aldrich).

Immunohistochemistry and Confocal Imaging Analysis

Mice were sacrificed, and the eyes were harvested on P21. The eyes were fixed using a special fixative solution (glacial acetic acid:formalin:0.9% sodium chloride:75% alcohol; 1:2:7:10), and 20 µm coronal sections of the eyes were prepared using a cryostat (Leica Microsystems). Tissue sections were incubated for one hour at room temperature in a blocking solution (10% bovine serum albumin plus 0.3% Triton X-100 in phosphate-buffered saline solution), followed by incubation with mouse polyclonal anti-rhodopsin antibody (1:2000; Millipore) at 4°C overnight. The sections were then washed in phosphate-buffered saline solution and incubated with goat anti-mouse TRITC-coupled secondary antibodies (ZsBio, 1:100) for two hours at room temperature. The nuclei were stained with Hoechst 33342 (Molecular Probes, Eugene, OR, USA, 1:5000). Images were acquired using a Zeiss LSM710META confocal microscope (Carl Zeiss AG, Oberkochen, Germany) and analyzed with ZEN 2009 Light Edition (Carl Zeiss AG) and Image-Pro Plus (version 6.0; Media Cybernetics, Rockville, MD, USA).

Quantification of the Retinal Layer Thickness

To quantify the thicknesses of the retina and the ONL, as well as the numbers of photoreceptor cells, 5 µm sagittal sections of eyes at different stages were prepared using a paraffin microtome (Leica Microsystems).The eye with optic nerve was aligned parallel to the blade on the paraffin microtome during sectioning. Sections were cut and chosen when the optic nerve is observed under microscopy. The pixel value across the murine retina was measured for each image of each mouse, and retinal and ONL thickness values were averaged for the central and peripheral regions of each group using ImageJ (National Institutes of Health, Bethesda, MD, USA).[31] All samples were measured in a blinded manner. The central part of the retina of each section was chosen for the quantification of photoreceptor cells. Using the software ImageJ, the nuclear architecture of photoreceptor cells on P14 was classified into two classes: (1) photoreceptor cells with fewer than three chromocenters and (2) photoreceptor cells with more than three chromocenters. The nuclear architecture of photoreceptor cells on P21 and P28 was classified into four classes: photoreceptor cells with (1) one chromocenter, (2) two chromocenters, (3) three chromocenters, and (4) more than three chromocenters. The nuclear architecture of photoreceptor cells at 6W was classified into two classes: (1) photoreceptor cells with one chromocenter and (2) photoreceptor cells with two chromocenters.

Light-Induced Behavior Analysis

Male C57BL/6, 129 × 1/svj, and ICR mice (aged 3–12 weeks) were used in this study. Mice were kept on a 12-hour light/dark cycle (lights on from 7:00 a.m. to 7:00 p.m.). All light-induced behavior tests were conducted during the dark period (9:00 p.m. to 12:00 a.m.). The temperature of the room was maintained between 22°C and 24°C. The behavioral experiments were conducted using a light-dark testing system (TSE Systems, Bad Homburg, Germany), which had two compartments: an open transparent compartment (light) and a closed black compartment (dark). A small door connecting the two compartments could be opened and closed automatically by the system. The light density in the light compartment was 200 lux. To facilitate adaptation, the animals were moved to the experimental room one hour before the test session.

The test was started by placing a mouse in the dark compartment for one minute. Then, the small door was opened for two minutes, and the mouse could move freely to the light compartment. Between experiments, both compartments were thoroughly cleaned with 70% ethanol, and the box was wiped dry with clean paper towels. This light-dark assay was performed according to the standard operating procedure from the Jackson laboratory. During this period, the walking distance of the mouse, the ratio of time with locomotor activity, mean velocity, percentage of mice exploring the light and dark compartments, percentage time of a mouse staying in the light compartment, latency before entering the light compartment after the door had been opened, and the visits of the mouse to the light or dark compartment were recorded by the TSE system (TSE Systems).

Blinding

Technically, the mice for staining are never "in experiment"; they are immediately sacrificed. Then, the technicians in our animal facility did paraffin sectioning and hematoxylin and eosin (H&E) staining. Students in the laboratory took the photos and performed the counting. All groups were named with Arabic numbers so the researcher would not know which group belongs to which one.

In light-induced behavior analysis, mice were put in the TSE machine, and then the machine recorded the activity of the mice automatically. This animal experiment was also performed by the technician in the animal facility. The main task was to put the mice in the machine, take the mice out of the machine, clean the machine, and put the mice back into the cage when the experiment was finished. The mice at the same age were divided into three groups, and all groups were named with Arabic numbers.

Statistical Analysis

All statistical analyses were performed using GraphPad Prism software 5.0 (GraphPad, San Diego, CA, USA). Parametric data were analyzed using a one-way analysis of variance with Tukey's post hoc test to correct for multiple comparisons. Nonparametric data identified with the Shapiro-Wilk test for normality were analyzed using the Kruskal-Wallis test with Dunn's correction for multiple analyses. All data are shown as the mean ± SEM, except light-induced behavior analysis, which was shown as the mean ± SD. Differences were considered significant if $P < 0.05$. In the light-induced behavior test, one-way analysis of variance was performed to analyze the data among different strains at the same time point in each metric. When the homogeneity of variances is more than 0.05, least significant difference post Hoc method is used, when the P value of the homogeneity of variances is less than 0.05, Tamhane's T2 post hoc test was used.

Results

The Thickness Values of the Retina and Outer Nuclear Layer Differed Among C57BL/6, 129 × 1/svj, and ICR Mice

On P21, the average thickness of the retina and ONL of C57BL/6 mice (202.76 ± 9.47 μm and 47.34 ± 2.14 μm, respectively) was greater than that of 129 × 1/svj mice (163.45 ± 3.38 μm and 39.57 ± 0.48 μm, respectively) (both $P < 0.05$). However, the average thickness values of the retina and ONL did not show statistically significant differences either between the C57BL/6 and ICR mice or between the 129 × 1/svj and ICR mice (Figs. 1D and 1E). The number of photoreceptor cells in ICR mice and C57BL/6 mice was 24% and 21% higher than that in 129 × 1/svj mice, respectively (both $P < 0.05$) (Fig. 1F).

On P21, the Percentage of Photoreceptor Cells With One Chromocenter is Increased in C57BL/6 Mice Compared to 129 × 1/svj and ICR Mice

In P14 mice, the percentage of photoreceptor cells with fewer than three chromocenters was in C57BL/6 mice, nearly 49% and 21% higher than that in 129 × 1/svj and ICR mice, respectively (both $P < 0.05$). The percentage of photoreceptor cells with fewer than three chromocenters was 22% lower in 129 × 1/svj mice than that in ICR mice (both $P < 0.05$). The percentage of photoreceptor cells with more than three chromocenters in 129 × 1/svj mice was nearly 7% higher than that in C57BL/6 mice ($P < 0.05$) (Figs. 2A and 2B). In P21 mice, the percentage of photoreceptor cells with one chromocenter was in C57BL/6 mice, nearly 86% and 333% higher than in 129 × 1/svj and ICR mice, respectively ($P < 0.05$). The percentage of photoreceptor cells with one chromocenter was increased by 133% in 129 × 1/svj mice compared to that in ICR mice ($P < 0.05$). No statistically significant difference was found in the percentage of photoreceptor cells with two chromocenters among C57BL/6, 129 × 1/svj, and ICR mice. The percentage of photoreceptors with three chromocenters was in ICR mice 100% and 33% higher than that in C57BL/6 and 129 × 1/svj mice, respectively

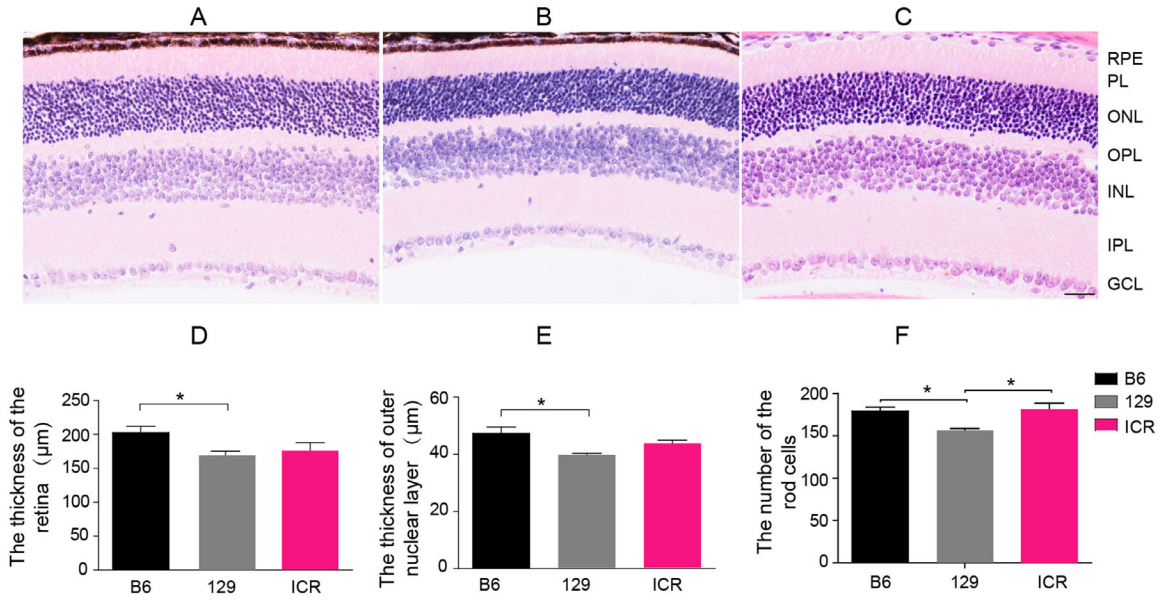

Figure 1. Thicknesses of the retina and the outer nuclear layer in C57BL/6, 129 × 1/svj, and ICR mice on P21. (A, B, and C) H&E staining images of the retina in C57BL/6 (B6), 129 × 1/svj (129), and ICR mice, respectively. (D and E) Comparisons of the retina (D) and outer nuclear layer (E) thickness in C57BL/6, 129 × 1/svj, and ICR mice. (F) The number of photoreceptor cells in C57BL/6, 129 × 1/svj, and ICR mice. RPE, retinal pigment epithelium; OPL, outer plexiform layer; INL, inner nuclear layer; IPL, inner plexiform layer; GCL, ganglion cell layer. *Scale bar*: 25 μm (n = 5 for each mouse strain). Data represent the mean ± SEM. $^{*}P < 0.05$ indicates statistical significance.

($P < 0.05$). However, no significant difference was observed between C57BL/6 and 129 × 1/svj mice. Similarly, the percentage of photoreceptor cells with more than three chromocenters was in ICR mice increased by 355% and 43% compared to that in C57BL/6 and 129 × 1/svj mice, respectively ($P < 0.05$). The percentage of photoreceptor cells with more than three chromocenters was in C57BL/6 mice 218% lower than that in 129 × 1/svj mice ($P < 0.05$) (Figs. 2C and 2D). In P28 mice, no significant differences in the four defined types of photoreceptor cells were observed among the three distinct strains of mice, except for the numbers of photoreceptor cells with three chromocenters in 129 × 1/svj and ICR mice, which were 100% and 120% higher than that in C57BL/6 mice ($P < 0.05$) (Figs. 2E and 2F). In six-week-old mice, photoreceptor cells were mature, and most of the photoreceptor cells had one chromocenter. The percentage of photoreceptor cells with one chromocenter showed no significant difference among the examined mouse strains (Figs. 2G and 2H).

Semi-Thin Sections Confirm the Percentage Differences in Photoreceptor Cells With One Chromocenter Among Mouse Strains on P21

Additionally, 0.5 μm semithin sections were used to determine the numbers of chromocenters in photoreceptor cells among the different strains of mice. Similar to the findings of the H&E staining, the percentage of photoreceptor cells with one chromocenter was on P21 significantly higher in C57BL/6 mice than that in 129 × 1/svj and ICR mice ($P < 0.05$). The percentage of photoreceptor cells with three or more chromocenters was in ICR and 129 × 1/svj mice significantly higher than that in C57BL/6 mice ($P < 0.05$) (Fig. 3).

Histone Distributions Confirm the Differences in the Architecture of Photoreceptor Nuclei Among the Three Mouse Strains on P21

The remodeling of the nuclear architecture of photoreceptors involves the movement of heterochromatin from the nuclear periphery to the center between P0 and P28, as well as the reduction in the number of chromocenters from several on P14 to one or two on P28.[7] On P21, the percentage of photoreceptor cells containing one chromocenter was in C57BL/6 mice significantly higher than that in 129 × 1/svj and ICR mice, and most photoreceptors in 129 × 1/svj and ICR mice contained more than three chromocenters. Therefore we determined on P21 the distribution of euchromatin (H3K4me3) and heterochromatin (H3K9me3 and H4K20me3) in photoreceptor cells of these three mouse strains. In C57BL/6 mice, the

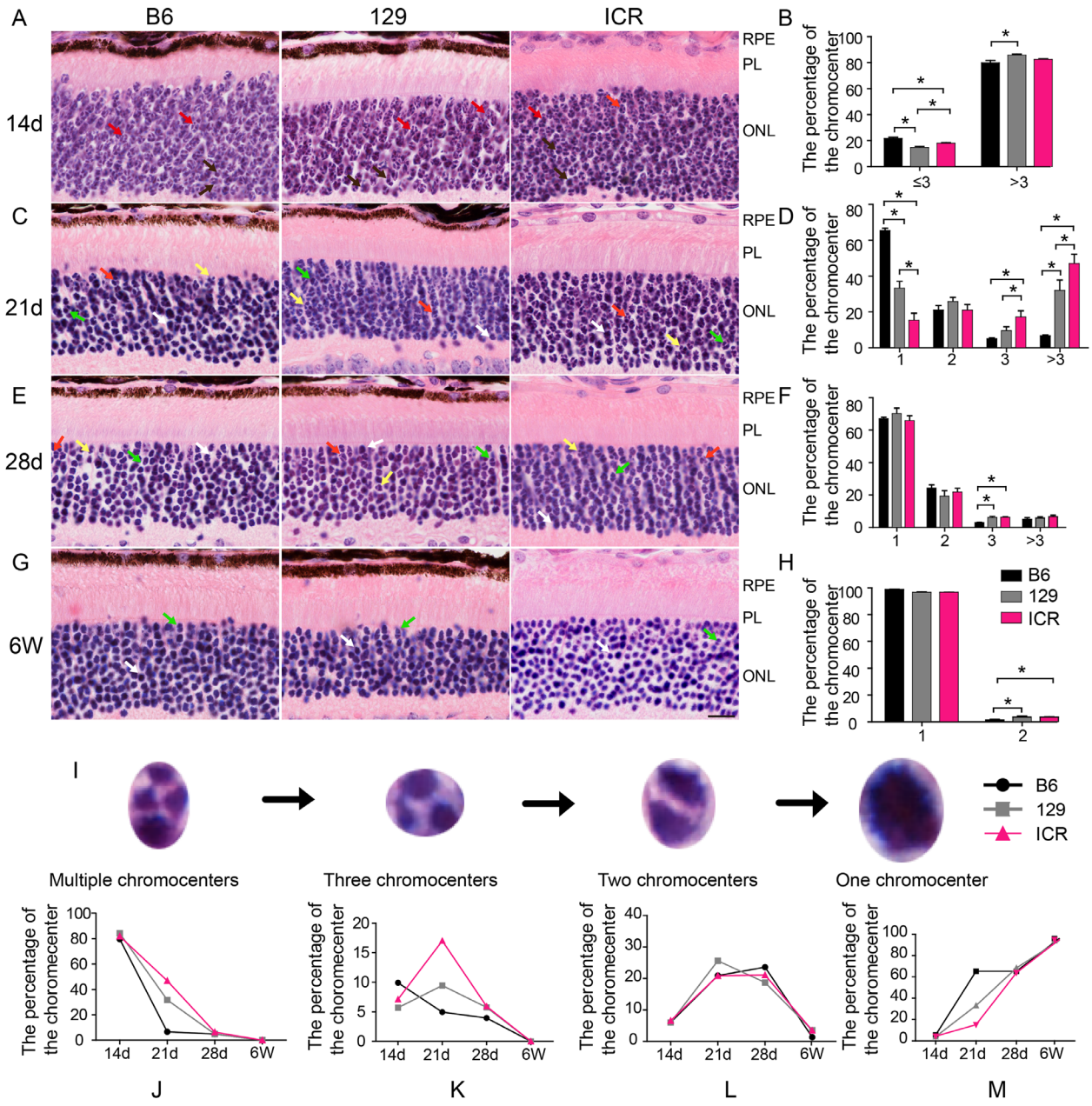

Figure 2. The nuclear architecture of photoreceptor cells in C57BL/6, 129 × 1/svj, and ICR mice at different ages. (A, C, E, and G) The nuclear architecture of photoreceptor cells in different mouse strains on P14 (A), P21 (C), and P28 (E), and at six weeks (G). (B, D, F, and H) Percentages of photoreceptor cells having more than three chromocenters, three chromocenters, two chromocenters, and one chromocenter in C57BL/6 mice, 129 × 1/svj, and ICR mice on P14 (B), P21 (D), and P28 (F), and at six weeks (H). (I) Schematic of the nuclear architecture of photoreceptor cells in C57BL/6 mice, 129 × 1/svj, and ICR mice at different ages. (J, K, L, and M) Percentages of photoreceptor cells with more than three chromocenters (J), three chromocenters (K), two chromocenters (L), and one chromocenter (M) from P14 to six weeks. *Red* and *black arrows* indicate photoreceptor cells containing more than three chromocenters and fewer than three chromocenters, respectively, on P14. *Yellow*, *green*, and *white arrows* indicate photoreceptor cells containing three chromocenters, two chromocenters, and one chromocenter, respectively. RPE, retinal pigment epithelium; PL, photoreceptor layer. *Scale bar*: 10 µm (n = 5 for each mouse strain at each time point). Data represent the mean ± SEM. $^{*}P < 0.05$ indicates statistical significance.

H3K4me3 euchromatin of nearly 64% of the photoreceptor cells was located at the periphery of the nuclei, whereas H3K9me3 and H4K20me3 heterochromatins were located in the central part of the nuclei in nearly 71% and 72% of the photoreceptor cells ($P < 0.05$) (Fig. 4A). In 129 × 1/svj and ICR mice, approximately 79% and 81%, respectively, of the H3K4me3 euchromatin in photoreceptor cells were located at

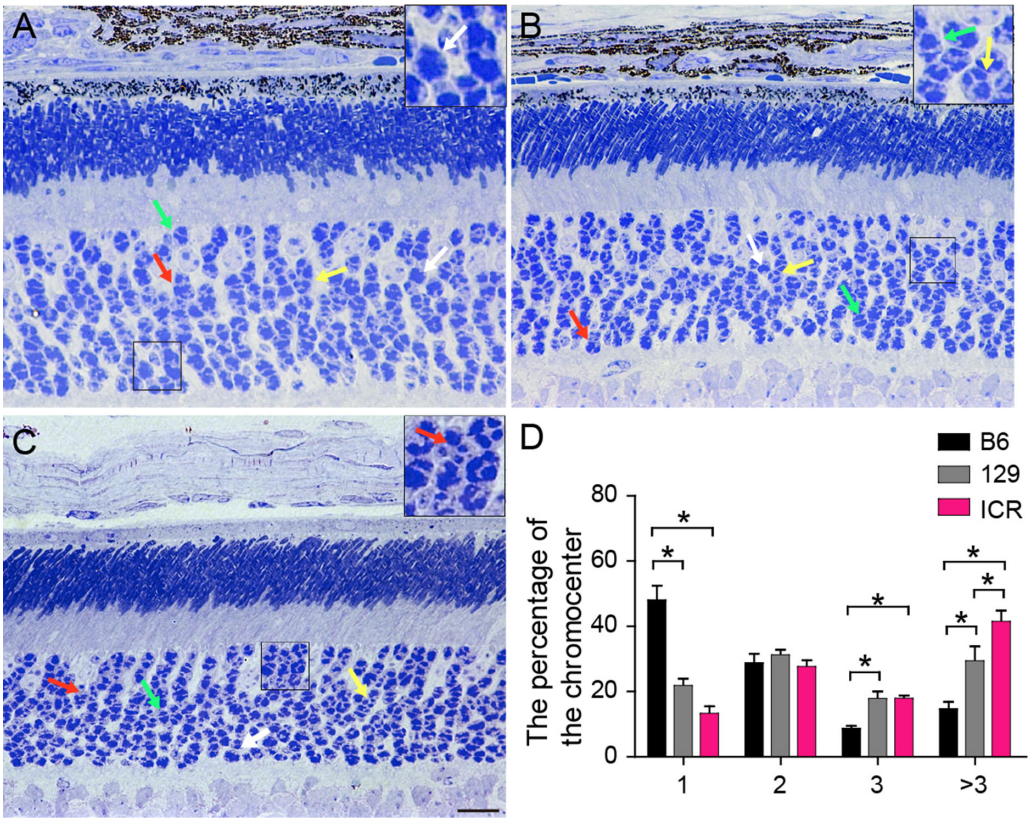

Figure 3. Ultrathin sections for the nuclear architecture of photoreceptor cells in C57BL/6 (B6), 129 × 1/svj (129), and ICR mice on P21. (A, B, and C) Nuclear architecture of photoreceptor cells in C57BL/6 (A), 129 × 1/svj (B), and ICR (C) mice. (D) Percentages of photoreceptor cells with more than three chromocenters, three chromocenters, two chromocenters, and one chromocenter. *Red arrows* indicate photoreceptor cells containing more than three chromocenters. *Yellow arrows* indicate photoreceptor cells containing three chromocenters. *Green arrows* indicate photoreceptor cells containing two chromocenters. *White arrows* indicate photoreceptor cells containing one chromocenter. *Scale bar*: 10 µm (n = 4 for each mouse strain). Data represent the mean ± SEM. $^{*}P < 0.05$ indicates statistical significance.

the center of the nuclei, whereas around 29% and 28% of H3K9me3 and 24% and 26% of H4K20me3 heterochromatin, respectively, were located at the center of the photoreceptor cell nuclei ($P < 0.05$) (Figs. 4C and 4E).

Expression of Rhodopsin and M-Opsin in the Three Distinct Mouse Strains on P21

Because the nuclear architecture of photoreceptor cells differed among the three mouse strains most remarkably on P21, the rhodopsin expression as a marker of rod photoreceptors was compared at this developmental stage. The expression level of rhodopsin was in C57BL/6 mice significantly higher than that in 129 × 1/svj mice ($P < 0.05$), whereas no statistically significant difference was noted between 129 × 1/svj and ICR mice (Figs. 5A and 5C).

We also compared the number of cone cells and the expression of M-opsin using DAB staining. The total number of cone cells was in ICR mice 24% and 23% higher than that in C57BL/6 and 129 × 1/svj mice, respectively ($P < 0.05$) (Figs. 5B and 5D). Cone cells were of two types: dot-shaped and rod-shaped. The number of rod-shaped cone cells was in ICR mice 25% and 23% higher than that in C57BL/6 and 129 × 1/svj mice, respectively ($P < 0.05$). By contrast, no statistically significant difference was detected in the number of dot-shaped cone cells among the three mouse strains.

Light-Induced Behavior of C57BL/6, 129 × 1/svj, and ICR Mice at Different Developmental Periods

The photoreceptor cells play essential roles in the day and night behavior of mice. Therefore the light-dark test was used to investigate the reaction of these different strains of mice to mild stressors such as light and new environments.[32]

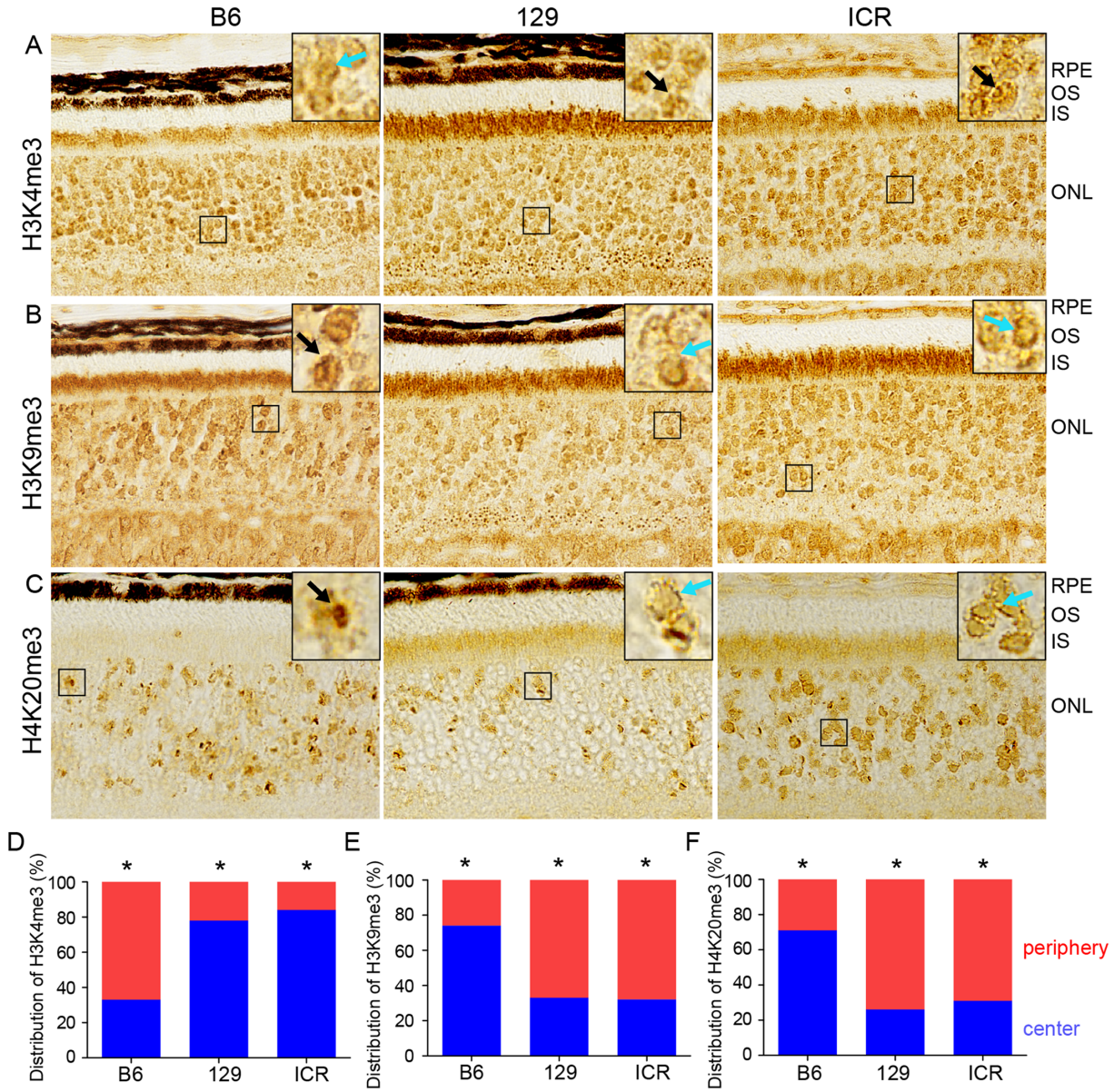

Figure 4. Distribution of marker histones in photoreceptor cells of C57BL/6 (B6), 129 × 1/svj (129), and ICR mice on P21. (A and D) H3K4me3 (euchromatin); (B and E) H3K9me3 (constitutive heterochromatin); and (C and F) H4K20me3 (heterochromatin). *Center*: histones located in the center of photoreceptor cells; periphery: histones located in the periphery of photoreceptor cells. *Green arrows* indicate histones located in the periphery of photoreceptor cells. *Black arrows* indicate histones located in the center of photoreceptor cells. RPE, retinal pigment epithelium; OS, outer segment; IS, inner segment. *Scale bar*: 10 µm (n = 4 for each mouse strain). Data represent the mean ± SEM. $^{*}P < 0.05$ indicates statistical significance.

In the light compartment, the walking distance, ratio of time for activity, velocity of activity, ratio of exploring area, the relative time of a mouse staying in the light compartment, and the average number of visits to the light compartment in C57BL/6 and ICR mice was significantly higher than that for 129 × 1/svj mice ($P < 0.05$) throughout the experiments, except for the tests at eight weeks and 12 weeks, whereas the parameter velocity of activity showed no significant difference and the test at 12 weeks, in which the ratio of time for activity indicated no statistically significant difference between C57BL/6 and 129 × 1/svj mice. The latency of a mouse entered the light compartment after the connecting door had been opened was significantly longer for 129 × 1/svj mice than for C57BL/6 and ICR mice at all time points ($P < 0.05$).

In the dark compartment, the walking distance, ratio of time for activity, velocity of activity, ratio

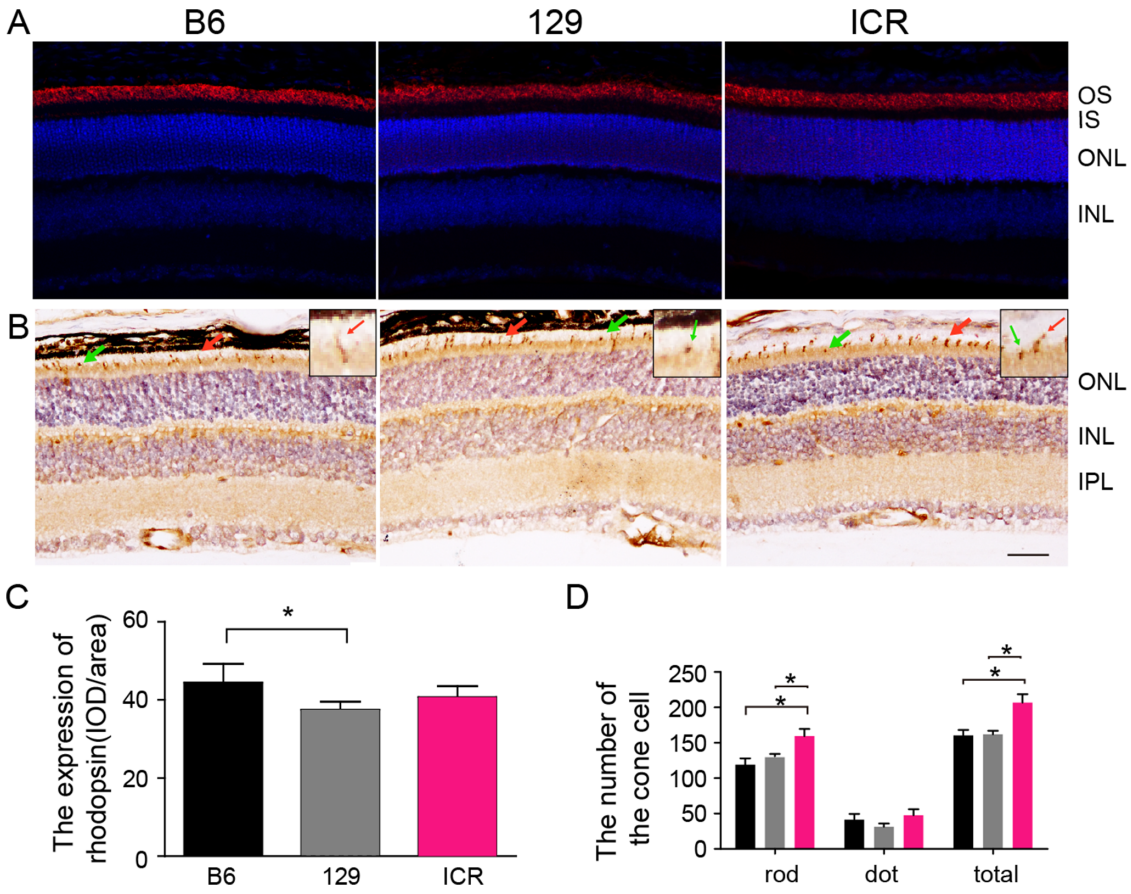

Figure 5. Expressions of rhodopsin and M-opsin in C57BL/6, 129 × 1/svj, and ICR mice on P21. (A) Immunostaining for the expression of rhodopsin in C57BL/6 (B6), 129 × 1/svj (129), and ICR mice. (B) DAB staining for M-opsin expression in retina sections of C57BL/6 (B6), 129 × 1/svj (129), and ICR mice. (C) Quantification of rhodopsin in C57BL/6, 129 × 1/svj, and ICR mice. *Scale bar*: 25 µm (n = 5 for each mouse strain). (D) Comparison of the numbers of rod-shaped and dot-shaped cone cells in C57BL/6, 129 × 1/svj, and ICR mice. *Red arrows* indicate rod-shaped cone cells. *Green* arrows indicate dot-shaped cone cells. OS, outer segment; IS, inner segment; INL, inner nuclear layer; IPL, inner plexiform layer. *Scale bar*: 50 µm (n = 5 for each mouse strain). Data represent the mean ± SEM. $^{*}P < 0.05$ indicates statistical significance.

of exploring area in C57BL/6 mice was significantly higher than that for 129 × 1/svj mice ($P < 0.05$) throughout the experiments, except for the tests at three, six, and 12 weeks, whereas the parameter walking distance showed no significant difference between C57BL/6 mice and 129 × 1/svj mice (Fig. 6 and Supplementary Data).

Discussion

This study demonstrated that three different strains of mice had distinct nuclear architectures of photoreceptor cells on P21 and different light-induced behaviors. This conclusion was based on the following results: (1) The findings of the H&E staining, semithin sections, and histone distributions all supported that the percentage of photoreceptor cells with one chromocenter was significantly higher in C57BL/6 mice than in 129 × 1/svj and ICR mice on P21. (2) The number of photoreceptor cells was significantly increased in ICR and C57BL/6 mice compared to 129 × 1/svj mice. Moreover, the total number of cone photoreceptors was significantly higher in ICR mice than in 129 × 1/svj and C57BL/6 mice on P21. (3) The thickness of the retina and ONL was significantly greater in C57BL/6 mice than in 129 × 1/svj mice. (4) ICR mice were more active than C57BL/6 mice, and C57BL/6 mice were more active than 129 × 1/svj mice in the light-induced behavior tests.

Solovei et al.[7] proved that the remodeling of the nuclear architecture of rod cells in nocturnal mammals was a process involving the transition from multiple chromocenters to one chromocenter, that is, four to six chromocenters on P14, one to three chromocenters on P21, one to two chromocenters on P28, and one chromocenter on W6. The same pattern was observed

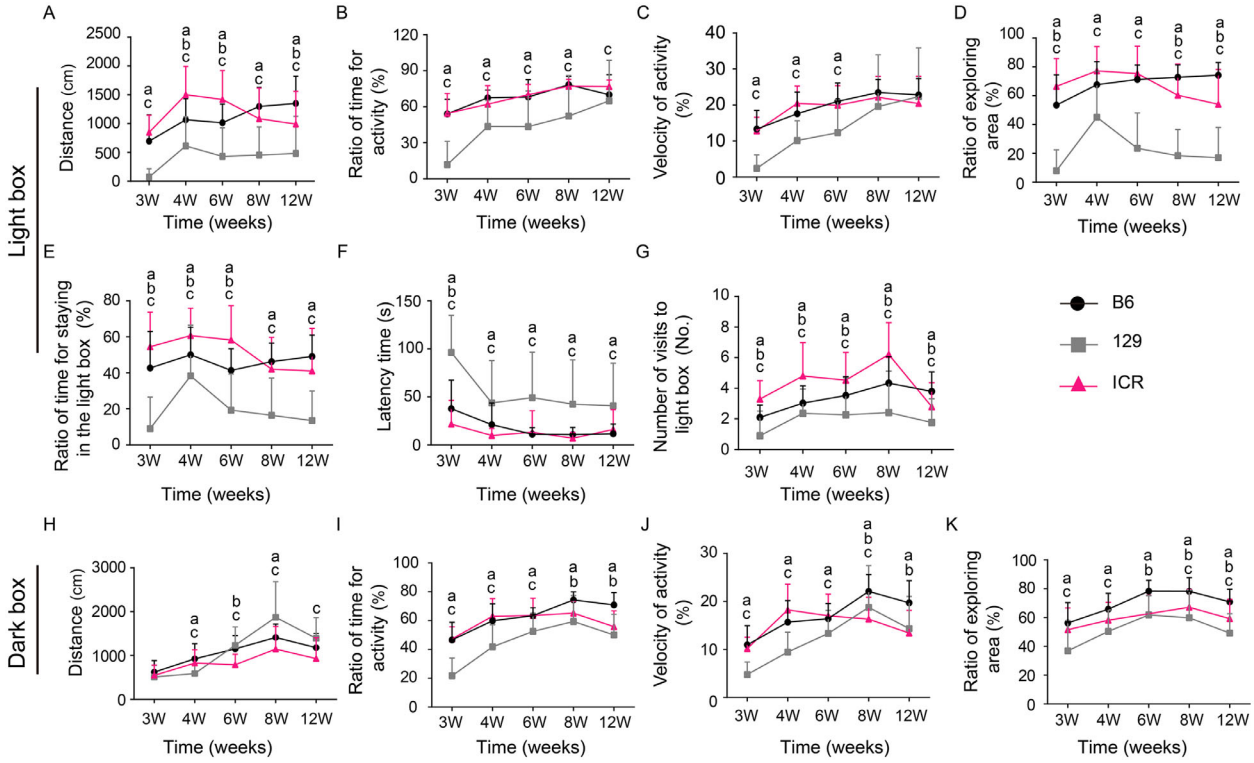

Figure 6. Light-induced behavior test of different developmental periods in C57BL/6 (B6), 129 × 1/svj (129), and ICR mice. (A) Walking distance of mice in the light compartment. (B) The ratio of time with locomotor activity in the light compartment. (C) The mean velocity of mice in the light compartment. (D) The percentage of mice exploring the light compartment. (E) The percentage of the time of a mouse staying in the light compartment. (F) The latency before entering the light compartment after the door connecting the two compartments had been opened. (G) The number of visits to the light compartment per mouse. (H) Walking distance of mice in the dark compartment. (I) The ratio of time with locomotor activity in the dark compartment. (J) The mean velocity of mice in the dark compartment. (K) The percentage of mice exploring the dark compartment. *a*, the significant difference between C57BL/6 and 129 × 1/svj mice; *b*, the significant difference between C57BL/6 and ICR mice; *c*, the significant difference between 129 × 1/svj and ICR mice (n = 30 for each mouse strain at each time point). Data represent the mean ± SD. $^{*}P < 0.05$ indicates statistical significance. One-way analysis of variance was performed to analyze the data among different strains of mice at the same time point in each metric. When the homogeneity of variances is more than 0.05, least significant difference post hoc method is used, when the *P* value of the homogeneity of variances is less than 0.05, Tamhane's T2 post hoc test was used.

in the present study, but the numbers of chromocenters in photoreceptor cells of C57BL/6, 129 × 1/svj, and ICR mice were different on P21. For C57BL/6 mice, nearly 70% of the photoreceptor cells had one chromocenter, whereas for 129 × 1/svj and ICR mice, nearly 40% and 65%, respectively, of photoreceptor cells had three or more chromocenters. This finding suggested that the photoreceptor cells in C57BL/6 mice matured earlier than those in 129 × 1/svj mice, which in turn matured earlier than those in ICR mice. The underlying reason might be that the localization and transcription activity of euchromatin and heterochromatin in photoreceptor cells differed significantly among these mouse strains. Indeed, we showed that in C57BL/6 mice, H3K4me3 euchromatin was detected in most photoreceptor cell nuclei periphery, whereas H3K9me3 and H4K20me3 heterochromatin staining were found in the center of most photoreceptor nuclei. In 129 × 1/svj and ICR mice, most of the H3K4me3 euchromatin was in the nuclei center, whereas H3K9me3 and H4K20me3 heterochromatin resided at the periphery of the nuclei of photoreceptor cells. This is in line with the study by Solovei et al.,[7] who showed that the heterochromatin of the rod photoreceptor cells of nocturnal retinas is situated in the nuclear center; however, euchromatin is located near the nuclear border. Several studies have shown that differences in the genetic background affect gene and protein expression in embryos, especially in the retina.[33–36] Kraus and colleagues[33] compared the gene expression pattern in 11 mouse strains, which are commonly used in transgenic mouse studies, such as C57BL/6J, 129 × 1/svj, S2/SvHsd, and Hsd: ICR(CD-1) mice on embryonic day 11.5 (E11.5), E12.5, and E13.5. Their

results showed that genes related to biological processes such as cell cycle, development, and stress response had significantly different expression patterns in these mouse strains on E12.5.[33] Jelcick et al.[34] investigated the differences in gene expression among AKR/J, CAST/EiJ, C57BL6/J, and NOD.NON-H2^{-nb1} mouse retinas on E18.5 and P30.5; their study revealed nearly 3000 differentially expressed genes among these three mouse strains.

In the present study, C57BL/6 mice had the highest mean retinal and ONL thickness values compared to 129 × 1/svj and ICR mice, and the difference was statistically significant. In agreement with this finding, Puk et al.[28] also demonstrated that the retina's thickness was significantly greater in C57BL/6 mice than in 129S2/SvJ mice. These morphological variations might result from different cell constitutions in the retina of different mouse strains. For instance, Kang et al.[37] demonstrated that the exclusive existence of specific cell types contributed to the thicker retina in C57BL/6 mice compared to 129/SvJ and BALB/C albino mice. The present study also found that the thickness of the ONL was increased in C57BL/6 mice compared to 129 × 1/svj and ICR mice. In addition, the numbers of photoreceptor cells were higher in ICR and C57BL/6 mice than in 129 × 1/svj mice. The expression level of rhodopsin was also significantly higher in C57BL/6 mice than in 129 × 1/svj mice. Moreover, the thickness of the inner nuclear layer and inner plexiform layer was significantly greater in C57BL/6 mice than in 129S2/SvJ mice (data not shown). Therefore the higher number of photoreceptor cells and the thicker ONL may partially account for the thicker retina in C57BL/6 mice.

The light-dark compartment test is designed to detect rodents' response to stressors based on the fact that mice possess an inborn aversion to light and new environments.[38] The current study investigated the light-induced behavior of these three mouse strains under the light-compartment condition on P21 (W3) and P28 (W4), and at six, eight, and 12 weeks. Under light- and dark-compartment conditions, C57BL/6 and ICR mice were more active than 129 × 1/svj mice throughout the experiments. Rod and cone photoreceptor cells are light-sensing cells in the mouse retina. Rod cells are predominantly responsible for retinal function under low-light or dark conditions, whereas cone cells activate and produce signals under brighter light conditions.[39–41] The numbers of photoreceptor cells in C57BL/6 and ICR mice were in the present study on P21 significantly higher than those in 129 × 1/svj mice. In addition, Patel et al.[42] demonstrated that photoreceptor structure, functional levels, and retinal thickness correspond to visual behavior. These findings may help explain why C57BL/6 and ICR mice were more active. The number of photoreceptor cells and the thickness of the retina were only examined on P21. However, studies have shown that the remodeling of the nuclear architecture of mouse photoreceptor cells is completed between P21 and P28,[7] the murine retina reaches morphological maturity on P21,[43] and the total thickness of the mouse retina does not change between two and six months of age.[28] Therefore the morphology and the number of photoreceptor cells on P21 may also represent the retina of these different mice strains on P28 (4 weeks), and at six, eight, and 12 weeks. Nevertheless, light-induced behavior remained significantly different across the three strains throughout the experiments. Thus other factors, such as genetic variations, neuronal maturation, and mice ability to explore new environments and deal with stress, might influence light-induced behavior in mice.[34,38] Therefore more suitable and sensitive tests should be developed to directly study the relationship between nuclear architecture and visual function. In addition, study showed that the expression of genes in response to aging is sexually divergent;[44] only male mice were used in this study, and therefore female mice should also be included in future studies.

Mouse models, with their well-established genetics and similarity to human physiology and anatomy, serve as powerful tools to investigate the etiology of human retinal diseases.[45] Genetically modified mice also provide reproducible experimental systems to shed light on the pathways of retinal function and development.[45] Therefore this study demonstrates a technique for assessing retinal structures, nuclear architecture, and light-induced behavior in various strains of mice, which are often used to model human retinal disease. Hence, this work may help to elucidate the effect of genetic or disease-induced variance in retinal architecture and the organization of photoreceptor nuclear content on visual function in humans.

Acknowledgments

The authors thank the technicians in the Animal Facility of Tsinghua University.

Supported by grants from the Radboud Institute for Molecular Life Sciences and Beijing Natural Science Foundation of China.

Disclosure: **M. Zhou,** None; **Y. Liu,** None; **C. Ma,** None

References

1. Kim JW, et al. Recruitment of Rod Photoreceptors from Short-Wavelength-Sensitive Cones during the Evolution of Nocturnal Vision in Mammals. *Dev Cell*. 2016;37(6):520–532.
2. Morshedian A, Fain GL. The evolution of rod photoreceptors. *Philos Trans R Soc Lond B Biol Sci*. 2017;372(1717):20160074.
3. Wang YV, Weick M, Demb JB. Spectral and temporal sensitivity of cone-mediated responses in mouse retinal ganglion cells. *J Neurosci*. 2011;31(21):7670–7681.
4. Carter-Dawson LD, LaVail MM. Rods and cones in the mouse retina. II. Autoradiographic analysis of cell generation using tritiated thymidine. *J Comp Neurol*. 1979;188(2):263–272.
5. Carter-Dawson LD, LaVail MM. Rods and cones in the mouse retina. I. Structural analysis using light and electron microscopy. *J Comp Neurol*. 1979;188(2):245–262.
6. Jeon CJ, Strettoi E, Masland RH. The major cell populations of the mouse retina. *J Neurosci*. 1998;18(21):8936–8946.
7. Solovei I, et al. Nuclear architecture of rod photoreceptor cells adapts to vision in mammalian evolution. *Cell*. 2009;137(2):356–368.
8. Shevelyov YY, Ulianov SV. The nuclear lamina as an organizer of chromosome architecture. *Cells*. 2019;8(2)136.
9. Jost KL, Bertulat B, Cardoso MC. Heterochromatin and gene positioning: inside, outside, any side? *Chromosoma*. 2012;121(6):555–563.
10. Postberg J, et al. Exploiting nuclear duality of ciliates to analyse topological requirements for DNA replication and transcription. *J Cell Sci*. 2005;118(Pt 17):3973–3983.
11. Van Bortle K, Corces VG. Nuclear organization and genome function. *Annu Rev Cell Dev Biol*. 2012;28:163–187.
12. Cremer T, Cremer M. Chromosome territories. *Cold Spring Harb Perspect Biol*. 2010;2(3): a003889.
13. Shachar S, Misteli T. Causes and consequences of nuclear gene positioning. *J Cell Sci*. 2017; 130(9):1501–1508.
14. Subramanian K, et al. Rod nuclear architecture determines contrast transmission of the retina and behavioral sensitivity in mice. *Elife*. 2019;8:e49542.
15. Acton JH, et al. Relationship between retinal layer thickness and the visual field in early age-related macular degeneration. *Invest Ophthalmol Vis Sci*. 2012;53(12):7618–7624.
16. Desmettre TJ. Epigenetics in Age-related Macular Degeneration (AMD). *J Fr Ophtalmol*. 2018;41(9):e407–e415.
17. Ho SM, et al. Environmental epigenetics and its implication on disease risk and health outcomes. *ILAR J*. 2012;53(3–4):289–305.
18. Nusinowitz S, et al. Retinal Structure in Pre-Clinical Age-Related Macular Degeneration. *Curr Eye Res*. 2018;43(3):376–382.
19. Friedman DS, et al. Racial differences in the prevalence of age-related macular degeneration: the Baltimore Eye Survey. *Ophthalmology*. 1999;106(6):1049–1055.
20. LaVail MM, Gorrin GM, Repaci MA. Strain differences in sensitivity to light-induced photoreceptor degeneration in albino mice. *Curr Eye Res*. 1987;6(6):825–834.
21. Polosa A, Bessaklia H, Lachapelle P. Strain Differences in Light-Induced Retinopathy. *PLoS One*. 2016;11(6):e0158082.
22. Tremblay F, et al. Prophylactic neuroprotection by blueberry-enriched diet in a rat model of light-induced retinopathy. *J Nutr Biochem*. 2013;24(4):647–655.
23. Matsumoto H, et al. Strain difference in photoreceptor cell death after retinal detachment in mice. *Invest Ophthalmol Vis Sci*. 2014;55(7):4165–4174.
24. Suzuki Y, Nakayama M. Differential profiles of genes expressed in neonatal brain of 129 × 1/SvJ and C57BL/6J mice: A database to aid in analyzing DNA microarrays using nonisogenic gene-targeted mice. *DNA Res*. 2003;10(6):263–275.
25. Gerlai R. Gene-targeting studies of mammalian behavior: is it the mutation or the background genotype? *Trends Neurosci*. 1996;19(5):177–181.
26. Kim JW, et al. Comparison of Adult Hippocampal Neurogenesis and Susceptibility to Treadmill Exercise in Nine Mouse Strains. *Neural Plast*. 2017;2017:5863258.
27. Williams RW, et al. Genetic and environmental control of variation in retinal ganglion cell number in mice. *J Neurosci*. 1996;16(22):7193–7205.
28. Puk O, de Angelis MH, Graw J. Longitudinal fundus and retinal studies with SD-OCT: a comparison of five mouse inbred strains. *Mamm Genome*. 2013;24(5-6):198–205.
29. Tkatchenko TV, Shen Y, Tkatchenko AV. Analysis of postnatal eye development in the mouse with high-resolution small animal magnetic resonance imaging. *Invest Ophthalmol Vis Sci*. 2010;51(1):21–27.
30. Zhou M, et al. The expression of a mitochondria-localized glutamic acid-rich protein

(MGARP/OSAP) is under the regulation of the HPG axis. *Endocrinology*. 2011;152(6):2311–2320.
31. Schneider CA, Rasband WS, Eliceiri KW. NIH Image to ImageJ: 25 years of image analysis. *Nat Methods*. 2012;9(7):671–675.
32. Paul KN, Saafir TB, Tosini G. The role of retinal photoreceptors in the regulation of circadian rhythms. *Rev Endocr Metab Disord*. 2009;10(4):271–278.
33. Kraus P, et al. Mouse strain specific gene expression differences for illumina microarray expression profiling in embryos. *BMC Res Notes*. 2012;5:232.
34. Jelcick AS, et al. Genetic variations strongly influence phenotypic outcome in the mouse retina. *PLoS One*. 2011;6(7):e21858.
35. Thiel R, et al. Time-dependent differences in the development of somites of four different mouse strains. *Teratog Carcinog Mutagen*. 1993;13(6):247–257.
36. Selman C, Swindell WR. Putting a strain on diversity. *EMBO J*. 2018;37(22).
37. Kang TH, et al. Comparative study of cholinergic cells in retinas of various mouse strains. *Cell Tissue Res*. 2004;317(2):109–115.
38. Bourin M, Hascoet M. The mouse light/dark box test. *Eur J Pharmacol*. 2003;463(1-3):55–65.
39. Peirson SN, et al. Light and the laboratory mouse. *J Neurosci Methods*. 2018;300:26–36.
40. Barnea-Cramer AO, et al. Function of human pluripotent stem cell-derived photoreceptor progenitors in blind mice. *Sci Rep*. 2016;6:29784.
41. Mustafi D, Engel AH, Palczewski K. Structure of cone photoreceptors. *Prog Retin Eye Res*. 2009;28(4):289–302.
42. Patel AK, Akinsoji E, Hackam AS. Defining the relationships among retinal function, layer thickness and visual behavior during oxidative stress-induced retinal degeneration. *Curr Eye Res*. 2016;41(7):977–986.
43. Brooks MJ, et al. Improved retinal organoid differentiation by modulating signaling pathways revealed by comparative transcriptome analyses with development in vivo. *Stem Cell Reports*. 2019;13(5):891–905.
44. Du M, et al. Retinal gene expression responses to aging are sexually divergent. *Mol Vis*. 2017;23:707–717.
45. Chang B. Mouse models for studies of retinal degeneration and diseases. *Methods Mol Biol*. 2013;935:27–39.